Measurement Science and Technology

PAPER • OPEN ACCESS

A delayed gating approach for interference-free ratio-based phosphor thermometry

To cite this article: Aldo Mendieta *et al* 2019 *Meas. Sci. Technol.* **30** 074002

View the article online for updates and enhancements.

You may also like

- Multi-spectral pyrometry—a review
António Araújo
- A New Method for Characterizing Very Low-Mass Companions with Low-Resolution Near-Infrared Spectroscopy
Emily L. Rice, Rebecca Oppenheimer, Neil Zimmerman et al.
- A NEW REDDENING LAW FOR M4
Benjamin Hendricks, Peter B. Stetson, Don A. VandenBerg et al.

This content was downloaded from IP address 202.8.112.224 on 05/07/2023 at 10:35

OPEN ACCESS
IOP Publishing
Measurement Science and Technology
Meas. Sci. Technol. **30** (2019) 074002 (9pp)
https://doi.org/10.1088/1361-6501/ab1b0c

A delayed gating approach for interference-free ratio-based phosphor thermometry

Aldo Mendieta, Benoît Fond, Plamen Dragomirov and Frank Beyrau

Institute for Fluid Dynamics and Thermodynamics, Otto-von-Guericke University Magdeburg, Magdeburg, Germany

E-mail: benoit.fond@ovgu.de

Received 24 January 2019, revised 1 April 2019
Accepted for publication 18 April 2019
Published 14 June 2019

Abstract

Accurate surface temperature measurements present vast difficulties in numerous technical applications, especially when imaging fast temperature changes. One example is spray-induced surface cooling, where temperature variations occur on the sub-millisecond timescale. Phosphor thermometry relies on changes in the photoluminescence properties (typically the lifetime or the emission spectrum) of phosphor materials for temperature determination. For temperature imaging in situations where short measurement durations are critical such as on fast moving objects or short and intense heat transfer events, the spectral method is preferred. However, in many situations, fluorescence signals over a broad spectral range originate from fuel, flame radicals, optical windows or even the chemical binder used to coat the phosphor material and may interfere with the measurements.

In this work, we investigate a delay strategy for the spectral method that prevents interference from fluorescence sources by using a phosphor with a microsecond-range-lifetime. By applying a short delay (<1 μs), between excitation and detection, short-lived interfering fluorescence signals can be efficiently avoided. The temporal and spectral content of the fluorescence from the substrate, binder and fuel are investigated with a photomultiplier tube and a spectrometer respectively. The delayed gating strategy is then implemented for temperature imaging of the wetted side of a spray impinged surface with a tin-doped phosphor, $(Sr,Mg)_3(PO_4)_2:Sn^{2+}$; selected for its suitable lifetime (26 μs @ 300 K) and high temperature sensitivity. Calibration measurements for coated surfaces show that by avoiding fluorescence from the binder, the temperature sensitivity is improved from 0.3% K^{-1} to 0.8% K^{-1} at 293 K. Furthermore the calibration curve repeatability between two similar coatings is enhanced. Finally, temperature measurements of the cooling induced by a fluorescing impinging gasoline spray was successfully performed with this strategy owing the same level of measurement precision (0.5 K) as with a non-fluorescing fuel (n-hexane UV grade).

Keywords: thermographic phosphors, laser induced fluorescence, gasoline, thermometry, impingement, fuel films

(Some figures may appear in colour only in the online journal)

Original content from this work may be used under the terms of the Creative Commons Attribution 3.0 licence. Any further distribution of this work must maintain attribution to the author(s) and the title of the work, journal citation and DOI.

1. Introduction

The access to detailed temperature information plays a key role in the analysis and conception of efficient thermal machines. However, performing precise temperature measurements still presents vast difficulties in a wide range of technical applications. This is particularly true in situations where the temperature strongly changes in time and space. Spray induced cooling in automotive applications is one example where local cooling appears near the point of impingement for only a short time.

Fast-response thermocouples with reported response times of around 1 μs can be used to capture fast temperature changes [16, 17, 20, 22, 26]. However, being point measurements, many closely spaced probes are necessary to correctly interpret the cooling pattern evolution thus an optical imaging technique is desirable.

Infrared thermography is another alternative. It allows for highly sensitive temperature measurements and is suitable for imaging of fast processes. For example, this technique was applied to analyse surface cooling on thin Inconel plates due to fuel spray impingement [25] for the analysis of surface heat-transfer improvement by using a special nanofiber coating [9]. However, reflected thermal radiations from surrounding surfaces [7] or radiation from a flame can strongly interfere with the measurements. Another issue with infrared thermography is the presence of a semi-transparent medium such as drops, for the detected spectral range [6] that can greatly affect the transmission of the thermal radiation to the detector.

Phosphor thermometry is another well-established approach. Thermographic phosphors are solid materials, which upon excitation, e.g. with UV light, emit light called luminescence. The photoluminescence properties (emission spectrum and lifetime) are temperature-dependent, and therefore remote thermometry can be performed by illuminating the phosphor and detecting its luminescence emission. Phosphor particles can be used for temperature measurement in fluids (in seeded form), see review [1]; or on surfaces, see review articles [2, 3, 5]. Two methods are normally followed to extract the temperature information. In the decay time method, the near-exponential temperature-dependent decay of the luminescence following pulsed excitation, is resolved by a fast detector. In this approach, the detector sampling rate must be sufficient to resolve the temporal decay, and the total measurement time is commensurate with the longest decay to resolve. For imaging, phosphors with decay times varying in the range of 10 μs to 5 ms are typically used, so that the full range luminescence decay can be resolved by a high-speed camera operating at 100's of kHz, and capable of recording 1000's frames per decay [13] or with the use of Photomultipliers [4, 19]. This approach allows sensitive and precise temperature imaging but reaches a limit when imaging fast temperature changes on the microsecond time scale.

In the spectral method, the temperature-dependent changes of the luminescence emission spectrum are exploited for thermometry using, frequently, a two-camera system with adequate spectral filters. With this approach, the measurement timescale is defined either by the camera exposure time, or by the luminescence lifetime of the phosphor, whichever is shorter. This approach is therefore the method of choice for fluid temperature measurements using the thermographic phosphor particles dispersed in the fluid, since a short exposure is needed to 'freeze the flow', see review [1].

In a recent work, Zinc oxide (ZnO) was coated onto thin steel plate to image the temperature resulting from the spray impingement [8]. Owing to the short $1/e$ lifetime below 1 ns [24], the measurement duration was limited by the laser pulse (10 ns), which was easily sufficient to resolve the rapid change in the surface temperature. A non-fluorescent fuel (n-hexane UV Grade) had to be used for these experiments because the fast fluorescence of real multi-component fuels interfered with the phosphor signal. However, it is clearly desirable to perform experiments with real, often fluorescing, fuels such as gasoline, more relevant to real-case scenarios. Moreover, other sources of interfering laser induced signals have been reported in phosphor thermometry experiments, such as the luminescence from windows, from the substrate, and/or from the chemical binder.

Since many of these interfering signals are short-lived, if a phosphor with a longer lifetime is used, it is possible to delay the exposure of the camera, and avoid these interferences altogether. This approach has been employed in the past for in-cylinder gas-phase temperature measurements to avoid the fluorescence from the window [23] or from gaseous reactive species [14, 15].

In this paper, we explore this strategy in the context of a spray impingement surface cooling application. A phosphor with a suitable decay time is chosen for this approach. The temporal dynamics and spectral content of the interferences are investigated. The impact of the interference on the measurement is then examined by comparing calibration curves obtained with and without delay (standard approach). Finally, as a demonstration, the surface cooling induced by a multi-component fluorescing fuel (gasoline) is measured.

2. Delay strategy and choice of phosphor

In many optical measurement applications, the light to be measured is generally combined with additional light signals, such as stray light, thermal radiation, fluorescence, which do not yield an exploitable relationship to the quantity of interest. To address this issue, spectral band-pass filters are normally used to improve on the selectivity of the targeted wavelength band of interest over the undesired interference bands. However, when the spectral content of useful and interfering signals overlaps, the interference is only partially reduced at the cost of a drop in useful signal. When using nanosecond pulsed excitation, selectively can also be performed in the temporal domain, by delaying and/or gating the exposure to discriminate between laser-induced signals of various lifetimes and continuous signals.

Phosphor materials cover a range of lifetime from nanoseconds to hours. Since the lifetime of laser-induced fluorescence signals is generally on the nanosecond scale, the signal from a phosphor with a decay time on the microsecond scale

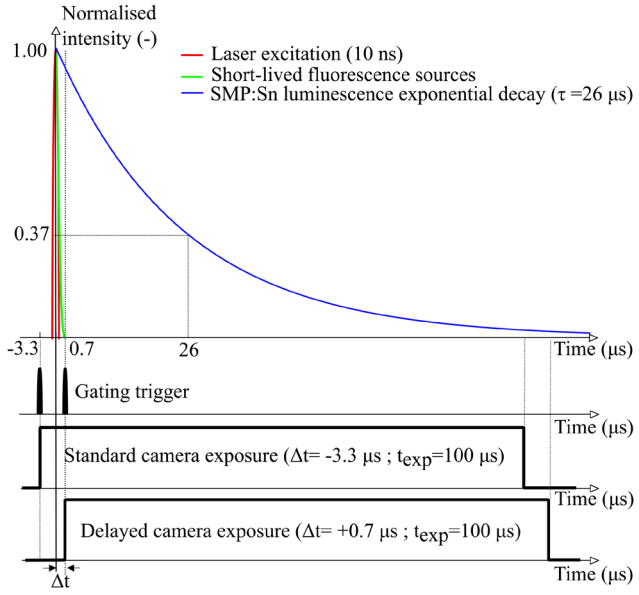

Figure 1. Schematic for the gating strategy. Differences between both triggering strategies are showcased as well as the the relative duration of the fluorescence sources, excitation laser and consequent $(Sr,Mg)_3(PO_4)_2:Sn^{2+}$ luminescence decay at room temperature ($T_{room} = 300\,K$).

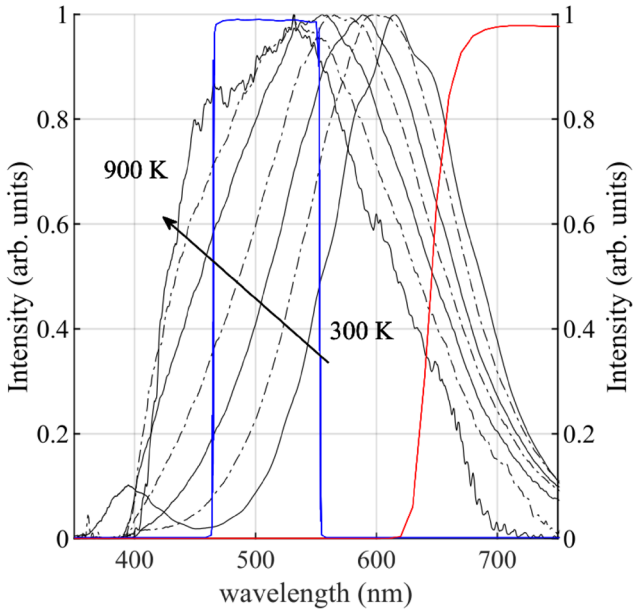

Figure 2. Normalised luminescence emission spectra of $(Sr,Mg)_3(PO_4)_2:Sn^{2+}$ particles (powder form) recorded from 300 to 900 K. Spectral filters 510-84 (blue) and RG645 (red) are also shown. Reprinted with permission from [11]. The Optical Society with permission of the Optical Society of America.

can be easily separated by delaying the camera exposure with respect to the laser pulse (see figure 1). Such strategy has been used in bio-imaging using nanophosphors to avoid auto-fluorescence from microorganisms. A mechanical gating system in the form of slotted chopper wheel was designed as a low cost add-on to a standard epifluorescence microscope to bypass auto fluorescence background signal for better visualisation of targeted microorganisms [18]. A 5 μs gating delay with a collection window of 320 μs @ 2.5 kHz was obtained.

The delayed gating strategy is intrinsically utilised in phosphor thermometry in the lifetime method where the sampled data is typically fitted over a time window which starts with some delay after the end of the excitation laser pulse. The different fitting algorithms as well as the acquisition temporal window definition is well explained in [12].

There are few reports of the use of a delayed exposure in phosphor thermometry with the intensity ratio approach, using intensified CCD cameras which offer a precise gating capability. For example, Hasegawa *et al* avoided laser induced fluorescence of combustion species when measuring gas temperature in a fired engine, using YAG:Dy^{3+} and applying a delay of 100 ns between the laser and the start of the 100 μs long exposure of an ICCD camera [14]. In another work by Neal *et al*, delays of a few microseconds were used when imaging the luminescence from YAG:Pr^{3+} in an optical engine but here with the additional aim to optimise the temperature sensitivity of the ratio of two emissions lines [23]. However this approach did not fully avoid the long-lived (>50 μs) luminescence of the windows.

To apply the delay strategy, the lifetime of the phosphor should be carefully considered. Assuming that the luminescence emission of the phosphor exhibits a single exponential decay with a time constant τ, and that the laser pulse duration is comparatively negligible, the expression for the fraction of total signal collected by an exposure of duration t_{exp}, starting at a delay Δt after the laser pulse is:

$$\frac{I}{I_{tot}} = e^{\frac{-\Delta t}{\tau}}\left(1 - e^{\frac{-t_{exp}}{\tau}}\right). \quad (1)$$

To maximize the first term, the decay constant should be long with respect to the delay necessary to avoid the fluorescence source. As shown in the second term, the exposure should be long enough to include a large portion of the luminescence decay. There is therefore a compromise between efficient rejection and short measurement duration. An additional consideration when using a delay strategy with a two-detector detection system is the jitter between the start of the exposure of both sensors which can cause the fraction of signal collected to vary between the two channels, and therefore induce measurement errors. This is not a problem with intensified CCD cameras, but for non-intensified interline transfer cameras, which are used in many studies for their low noise characteristics, jitters of several 10's of nanoseconds were reported [10].

In this study we choose, $(Sr,Mg)_3(PO_4)_2:Sn^{2+}$, referred in the following as SMP:Sn, a phosphor which was recently characterized for fluid thermometry [11]. The authors reported a 1/*e* luminescence lifetime is 26 μs at 300 K and a temperature sensitivity, using the spectral filters described below (see figure 2), of ~0.6% K^{-1}. The sensitivity was similar to that reported in the abovementioned study with ZnO coatings [8]. The emission intensity per particle, which was measured in liquid dispersions, is also similar to that of ZnO.

Using a delay of 700 ns and an exposure of 100 μs (see figure 1), more than 95% of the signal is collected. In addition, a jitter in the camera gating of 50 ns would result in a

negligible 0.2% variation in the ratio of the gathered signal (translating to a 0.3 K variation at 300 K based on the aforementioned sensitivity). As a result, using this phosphor with the described delay strategy will allow rejection of the fluorescence signal while maintaining a relatively short measurement duration and a high measurement precision. An additional advantage of using the tin-based phosphor is the 10-fold reduction in cross-sensitivity to the excitation fluence in comparison with ZnO, which relaxes the constraints of an inhomogeneous fluence over the phosphor coating surface. On the other hand, $(Sr,Mg)_3(PO_4)_2:Sn^{2+}$ can only be efficiently excited at 266 nm (using a Nd:YAG pulsed Laser). The switch from 355 nm excitation previously used with ZnO to 266 nm for the tin-based phosphor potentially leads to increased fluorescence signal intensity, since fluorescence in gasoline is dominated by aromatic components, mostly naphthalene [21], which presents stronger UV absorption between 200–300 nm than in the 300–400 nm region. Therefore stronger fuel fluorescence is expected under 266 nm excitation than 355 nm excitation.

In the following we investigate the improvements upon the application of the delay strategy in temperature measurements of surfaces subject to fuel spray impingement.

3. Experimental setup

3.1. Phosphor coating

Two steel plates (100 mm × 60 mm × 0.5 mm) were spray coated with a suspension of binder (*Ofenfarbe, ULFALUX*), thinner and SMP:Sn particles. The proportions of phosphor, binder and thinner were 500 mg: 100 ml: 25 ml respectively. After the spray deposition, all coated plates were annealed in an industrial oven at a 150 °C temperature for around 12 h. More details on the preparation procedure can be found in [8].

After annealing, coatings *a* and *b* had averaged thicknesses of 22 μm and 22.8 μm respectively determined by measurements of the total thickness before and after the coating procedure in 4 different points of the coated plate and substrate surface using a standard screw micrometre (Mitutoyo, MDC-1″ PJT). Additionally, another plate was coated with a similarly thick coating using only the chemical binder to examine more closely the binder fluorescence emission characteristics.

3.2. Spectroscopy of the fluorescence sources

To validate the use of the gating strategy, important data about the lifetime and spectral content of the fluorescence of the different participating sources has to be analysed. For this, four targets were used and illuminated with UV excitation: an uncoated plate, a plate coated with binder only, an uncoated plate covered by a film of gasoline, and an uncoated plate covered by the phosphor in powder form.

To examine the temporal decay of the fluorescence, the targets were illuminated by the output of a pulsed (10 ns duration), frequency quadrupled, Nd:YAG laser (Quanta-Ray GCR-150, Spectra-Physics) at 266 nm operating at 15 Hz with a fluence of approximately 0.06 mJ cm^{-2} and the signals

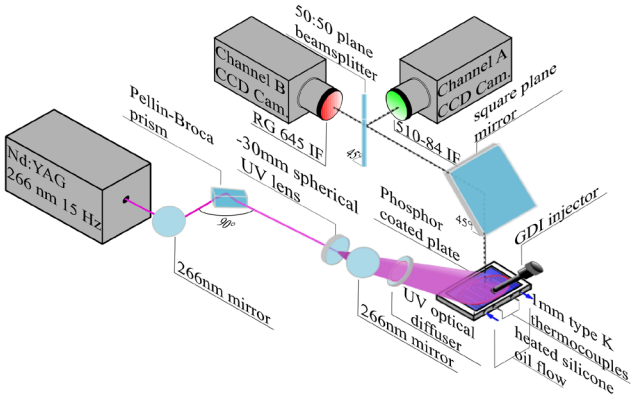

Figure 3. Experimental setup for impingement surface cooling measurements. Two CCD cameras, equipped with interference filters, RG 645 and 510-84 (CWL-FHWM), detect the spectrally filtered luminescence signal from the $(Sr,Mg)_3(PO_4)_2:Sn^{2+}$ coated plate. 15 Hz is the repetition rate of both the excitation signal and the acquisition.

were gathered by a Photomultiplier—PMT—(Hamamatsu R955HA) and read out by a digital oscilloscope (Tektronix MDO3034, 350 MHz). Note that for practical reasons (higher sensitivity of the PMT), a lower excitation fluence was used for the qualitative temporal and spectral analysis of the interfering signals than for the actual thermometry experiments. For quantitative evaluation, the same fluence should be used in case there is a dependency of the temporal and spectral content of these signals on the excitation fluence.

An input impedance of 75 Ω between the PMT and the oscilloscope lead to a fall time of 30 ns. The sampling rate was set to 2.5 Giga samples s^{-1}.

The luminescence from the targets was also imaged onto the entrance slit of a spectrometer (Acton Research SP300i, $f = 500$ mm, 300 grooves mm^{-1}) with a 50 mm *f*/1.4 Nikon lens in combination with a CCD camera (Imager Pro-X, LaVision, 1600 x 1200 pixels) covering a spectral range of 120 nm. To cover a wider range, measurements were performed at two central wavelengths (470 nm and 600 nm). The entrance slit was set to 0.1 mm corresponding to a spectral resolution of 1 nm. A 295 nm long-pass colour glass (WG295) helped filter out 266 nm laser light.

To visualise the broadband characteristics of the binder, and gasoline film, no delayed gating strategy was used, gating the cameras exposure before the laser trigger. For the SMP:Sn phosphor, the gating strategy was applied. The camera exposure was set in all cases to 100 μs. A mercury and a tungsten lamp were used for pixel spectral scaling and throughput calibration respectively of the spectrometer.

3.3. Two-dimensional thermometry setup

To examine the impact of the delay strategy on the measurements, a 2D measurement system illustrated in figure 3 was used. The coating was excited by the an expanded laser beam formed by means of a diverging spherical lens ($f = -30$ mm) and a 5° beam diffuser window (48-515, Edmund Optics) to

further homogenise the laser fluence distribution. The fluence was set to 0.4 mJ cm^{-2}. A Pellin-Broca prism was used to filter out the residual 532 nm output from the laser. The luminescence, reflected by a UV-enhanced mirror (Edmund Optics 84428), is split using a spectrally-flat beamsplitter (Edmund Optics 46-642). The reflected and transmitted signals are later collected by two, 2 × 2 hardware binned, CCD cameras (Imager Pro-X, LaVision) equipped with 85 mm *f*/1.4 lenses (Carl-Zeiss) operating at 15 Hz. A field of view of 105 mm by 80 mm was obtained with a resolution of 800 × 600 pixels. Each lens had spectral filters attached to exploit the blue-shift of the phosphor emission band with increasing temperature. A long pass colour glass (Schott RG645) is attached to camera 1 and a bandpass 510–84 nm filter (Edmund Optics 84-113) in CWL-FWHM notation (Center Wavelength—Full Width at Half width Maximum) is used on camera 2, as depicted in figure 3. The standard strategy used a negative exposure delay $\Delta t = -3.3$ μs, whereas the delayed strategy used a positive exposure delay of $\Delta t = +0.7$ μs, with the laser pulse as a reference. The exposure duration was held constant at 100 μs (see figure 1). Shorter exposures can also be used at the expense of lower signal gathering to further reject undesired long-lived background interference. For example, using the same SMP:Sn phosphor, reducing the exposure to 50 μs and 10 μs yields a total signal collection of 83% and 31%, respectively (applying the same positive exposure delay $\Delta t = +0.7$ μs).

The acquired luminescence images were background subtracted and white-field corrected (using the room temperature calibration field) and smoothed using a 7 × 7 pixel moving filter for a final effective resolution of 0.9 mm similar to the setup described in [8].

3.4. Calibration procedure

A five-step temperature calibration process, ranging from room temperature (≈292 K) to 493 K, was performed *in situ* for each coated plate. Each temperature point was evaluated over 100 shots and later averaged. The plate was clamped on top of a thick aluminium body with a machined trench as to form a serpentine-shaped channel through which silicon oil flew in direct contact with the underside of the coated plate. The silicon oil was supplied by a temperature controlled silicon oil bath in a closed loop. Temperature was continuously monitored by means of two thermocouples (see figure 3). Those were inserted into the aluminium body and positioned 5 mm below the contact point of the aluminum body with the steel coated plate.

Modelling steady state heat transfer with thermal resistances, the temperature deviation between the top of the coating and the thermocouple was estimated to be less than 0.5 K (at 393 K surface temperature).

3.5. Gasoline direct injection system

To demonstrate the capability of the delayed strategy, the temperature imaging system was applied to measure the cooling induced by the impingement of high pressure spray of a multi-component gasoline fuel.

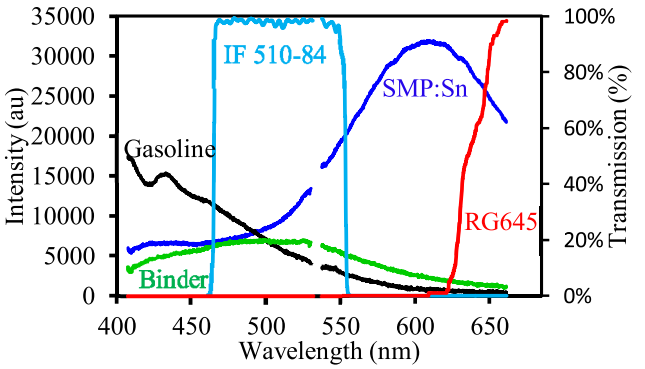

Figure 4. Spectrometer measurements (taken at 300 K) for the luminescence spectra of the main sources of interference and for the tin-doped phosphor coating using 266 nm excitation. Filter transmission as a function of wavelength is also shown.

A gasoline direct injection (GDI) injector (BOSCH—HDEV 5.2) was used with two different fuels; a reference gasoline and a non-fluorescence UV grade n-Hexane (T908.1, Carl Roth). The injection nozzle was positioned 35 mm over the coated plate and the injector body tilted 30° from the vertical. Both fuels were injected at a 15 MPa (±0.5 MPa) rail pressure, using a mechanical pressure amplifier, using a Nitrogen based high pressure tank for stable pressure injection minimising pressure drop at the rail during injection.

A standard gasoline direct injection ECU (engine control unit) system was used to precisely control the timing and triggering of the injector using the signals coming from the laser trigger as reference, applying different delays for the start of the acquisition (taking the start of injection as a reference). Using a high speed camera as described in [8], and triggering the 10 kHz recording with the injector input trigger signal, the start of the injection was observed on the same frame for each injection. The jitter of the injection unit was therefore estimated to be below 100 μs.

4. Measurement results

4.1. Spectral analysis

The spectral content of the emission from the various sources, using 266 nm laser excitation, are shown in figure 4. Both the binder and gasoline fluorescence exhibit spectrally broad emission extending from the UV to red region of the light spectrum. For gasoline, the strongest intensities are observed in the near-UV region, which decrease towards the red region. The spectrum of the binder fluorescence, show a relatively flat intensity over the blue green and yellow regions of the visible spectrum. For comparison, the emission spectrum of the phosphor-coated plate, and the filter bands used for the thermometry are also shown. Due to the significant overlap, and the fluorescence spectra of gasoline and the binder, fluorescence cannot be efficiently rejected spectrally, without significantly affecting the useful phosphor signal.

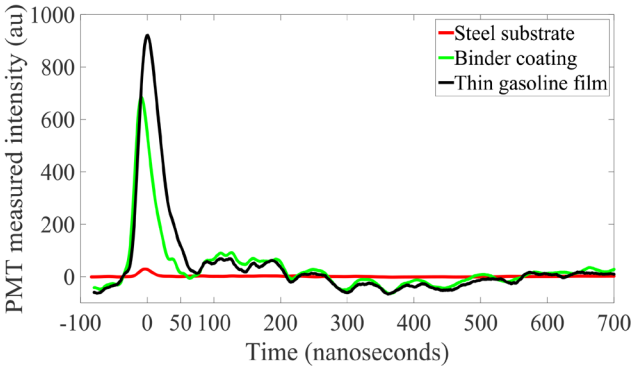

Figure 5. Temporal evolution of the laser induced fluorescence from the different probed elements. A WG 295 filter was used to filter out any 266 nm scattered light.

As noted in figure 4, much more influence of the gasoline and binder fluorescence is noted in the 510–84 nm filter compared to a much lower gathered signal in the RG645 filter. Note that on figure 4, the spectral range from 529–537 nm is missing to avoid damaging the detectors with residual 532 nm laser emission, since a Pellin-Broca prism was not used during the spectral measurements.

4.2. Temporal measurements

Decay curves observed for the different targets are shown in figure 5. Here the raw absolute intensity is shown to assess the relative intensities of the fluorescence signals. The longest-lived signal was observed for gasoline, reaching 10% of the initial intensity after 70 ns. The binder fluorescence, decayed more rapidly although with a similar intensity as the fuel film. For the substrate, much weaker signals coming from the metal itself or deposited dust particles are observed. By comparing the intensity of those signals with and without a 532–10 nm narrow bandpass filter, it was verified that the signals resulting from scattered green residual laser light are negligible in comparison to the other sources. Note that in figure 5, the temporal characteristics of the binder and gasoline emission are convoluted with the response time of the detection system (~30 ns) so that the fluorescence signals are in reality shorter-lived than they appear here. Therefore a delay of 100's ns should be largely sufficient to completely bypass the contribution of those undesired signals, even taking into account the laser-camera exposure jitter.

These measurements indicate that using a delay of several 100's of ns would eliminate completely the contribution of those undesired signals.

4.3. Temperature response comparison for both strategies

The calibration curves obtained for two very similar coatings are shown for the delayed and non-delayed (standard) strategies in figure 6. The horizontal error bars correspond to the error in the reference temperature (~1 K), and the vertical error bars correspond to the statistical uncertainty (maximum and minimum values obtained during measurement).

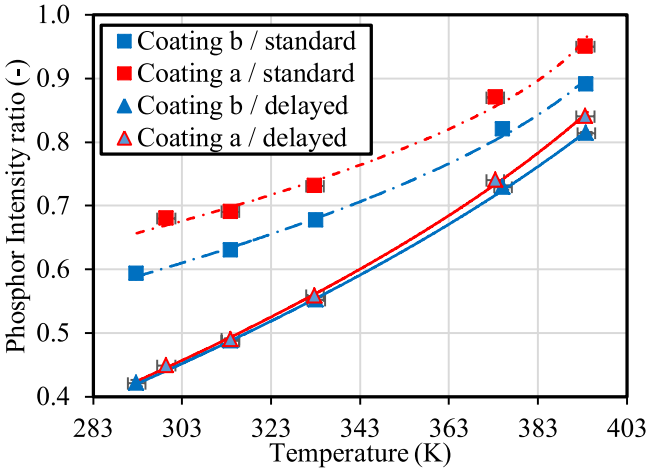

Figure 6. Calibration of the intensity ratio as a function of temperature (measured by thermocouples) for coatings a and b. A quadratic function fit (see equation (2)), represented by the dashed (standard strategy) and full (delay strategy) curves is applied to all cases. Temperature (horizontal) and PIR (vertical) error bars are superposed to the calibration points.

The first observation is that at all temperatures and for both coatings, the intensity ratio is significantly lower with delaying than without, which is in agreement with a stronger spectral contribution of the binder fluorescence in the channel with the 510–84 nm filter (see figure 4). The deviations between the calibration curves obtained with the two strategies decreases with higher temperatures and this is true for both coatings.

To shed some light into this latter observation, the temperature response of the binder only coated plate was analysed using the same experimental setup represented in figure 3. Results, shown on figure 7, indicate that the binder fluorescence signals in each channel decrease with temperature, due to thermal quenching. On the other hand the luminescence emission intensity of SMP:Sn is only very weakly temperature dependent over the 300–400 K range, as reported in [11]. Therefore, at higher temperatures the contribution of the binder fluorescence is lower and a better agreement is observed between the intensity ratio versus temperature curves obtained with both strategies.

Another striking feature in the comparison of calibration curves obtained with the standard and delayed strategy, shown in figure 6, is that for the standard strategy, the calibration curves between the two coatings is noticeably different. This would indicate a different contribution of the binder luminescence between the coatings. This effect requires the use of individual calibration curves for each coating in practical measurements. When applying the delayed strategy, the two curves (coatings a and b) overlap well, with the maximum ratio difference translating to an error of less than 5 K (0.76 versus 0.79 in the ratio for the 393 K calibration point). This indicates that the requirement for individual temperature calibration may be potentially lifted with the delayed strategy. Spatial pixel-to-pixel precision (standard deviation), averaged over 100 shots, of the mean surface temperature, ranged from 0.4 K to 0.8 K, for 292 K and 393 K respectively, with the delayed strategies.

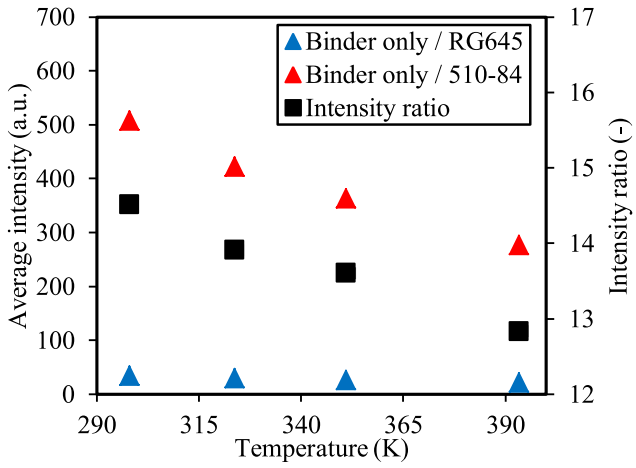

Figure 7. Absolute signal intensities (after background subtraction) collected in channels A and B for a pure binder coating (no phosphor added). The ratio between both channels is also shown.

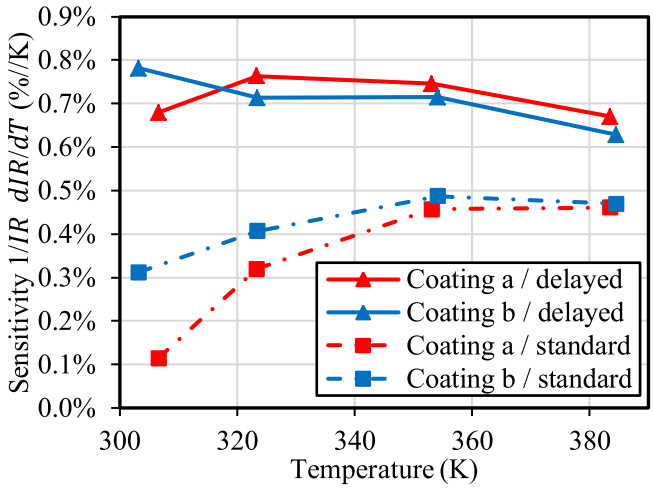

Figure 8. Temperature sensitivity as a function of temperature shown for coatings a and b comparing the impact of both gating strategies.

A second order polynomial was fitted to the measured calibration points (equation (2)) obtained with the delayed strategy. In this equation T and PIR are the temperature in Kelvin and dimensionless phosphor intensity ratio respectively, and a, b and c are arbitrary constants defined by the fitting algorithm

$$T\ (\mathrm{K}) = a \times \mathrm{PIR}^2 + b \times \mathrm{PIR} + c. \qquad (2)$$

The fractional temperature sensitivity was derived numerically as the relative rate of change between two consecutive data points of figure 6 to which we assign the mean of the two temperatures. The results in figure 8 show that at room temperature, the temperature sensitivity with the delayed strategy is more than 2 times higher than with the standard strategy for either coating. This improvement in the sensitivity can be understood by examining the temperature response of the intensity ratio measured for the plate coated only with binder, shown in figure 7. As opposed to the phosphor behaviour, with increasing temperature the binder fluorescence in the RG645 channel increases relative to that in the 510–84 nm channel

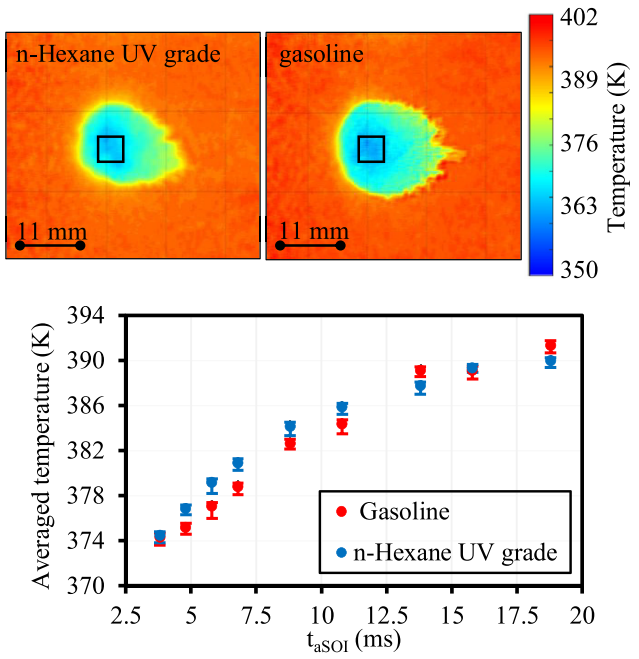

Figure 9. (Top) Surface temperature fields (in K), acquired at 3.8 ms aSOI for coating a, at 395 K initial temperature, using n-Hexane (UV grade) and gasoline, at 292 K. A delay of 0.7 µs was applied in both cases. (Bottom) Spatially averaged (black frame on top figures) temperature evolution for different instants after the start of injection, including error bars.

with an average temperature sensitivity of 0.12% K^{-1}. The intensity ratio (510-84/RG645) of the binder fluorescence and that of the phosphor luminescence have opposing trends with increasing temperature. The first decreases, while the second increases. When both signals are convoluted, the increase of the ratio of the phosphor luminescence with increasing temperature is compensated by the decrease of the binder fluorescence ratio (see figure 7), and as a result the temperature sensitivity (fractional increase in the intensity ratio) is lower than for the phosphor luminescence alone.

4.4. Spray induced cooling measurements

The instantaneous temperature field measured 3.8 ms after the start of injection (aSOI) for gasoline and the fluorescence-free fuel (n-Hexane), both at room temperature (292 K) with an GDI injector operating at 150 bar and 1.9 ms excitation time, are shown on figure 9 (top). During these measurements, using coating a, a temperature of 395 K was initially set. At this time, fuel films are still present, as observed by [8], using direct photography of the n-Hexane film with a high-speed camera. Both figures show no noticeable artefacts caused by interference from fuel fluorescence, either from n-Hexane UV grade or especially from gasoline. Slight differences can be observed though, that may be due to the different physical properties of the tested fuels.

Fine detail can be observed in the film front which indicates the high spatial resolution of these cooling measurements performed from the wetted side of the wall, while in IR measurements performed on the dry side of the wall (oppose

to the impinged face), axial conduction heat transfer contributes to significant blurring of the cooling pattern, see [25].

Lastly, measurements were performed at different times after the start of injection for each fuel (gasoline and UV grade n-Hexane), and the measured temperature was spatially-averaged within a 5 × 5 mm area represented by the black frame in figure 9 (top). To estimate the temperature precision of the measurements, 90 single shot measurements were recorded under stable temperature conditions (at 292 K and 340 K) prior to injection. The single shot pixel to pixel standard deviation was calculated to be 0.4 K and 0.6 K at 292 K and 340 K, respectively. The vertical error bars correspond to the statistical uncertainty (maximum and minimum values obtained during measurement). As shown in figure 9 (bottom), the reheating of the plate, after a few milliseconds of the impingement, follows a similar pattern for both tested fuels.

5. Conclusions

In this work, a delay gating strategy is proposed as a way to avoid interferences from fast decaying fluorescence interference signals when using the phosphor intensity ratio approach for surface thermography and implemented to a fuel-spray-impingement cooling test-case.

A tin-doped phosphor ($(Sr,Mg)_3(PO_4)_2:Sn^{2+}$), which was found in a recent study to yield high temperature sensitivity, was used in this work. Its lifetime of 26 μs allowed using a positive delay of the exposure with minimal signal loss.

The spectra of laser induced fluorescence emission from the substrate, binder and gasoline film were found to span several 100's of nanometers preventing efficient rejection with spectral filters. However, the stronger interference signals (gasoline and binder) were found to decay within 100 ns, and a detector delay of 700 ns was chosen for complete suppression. This corresponds to a negligible 5% signal loss in phosphor luminescence emission.

The temperature responses of both standard and delay strategies were examined for two coatings. The temperature sensitivity was shown to improve by a factor of two at 293 K with the delay strategy. Considering the lack of information regarding fluorescence characteristics of chemical binders and/or contamination from other sources, this strategy can be of great utility by other researchers in the phosphor surface thermometry field.

In addition, discrepancies between calibration curves obtained with two very similar coatings were significantly reduced with the delay approach. This could in principle allow *ex situ* calibration with a reference coating. This would allow calibration in setups such as transparent engines, where performing *in situ* calibration at specific, controllable and spatially homogeneous temperatures is often not possible. Finally, using a gasoline direct injection system, surface spray-cooling measurements using reference (fluorescing) gasoline and fluorescence-free n-Hexane were performed. Precise instantaneous temperature measurements following spray impingement were obtained from the wetted side and through the liquid film for both fuels.

In summary, by allowing measurements with 'real' fuels, potential for *ex situ* calibration, and a higher temperature sensitivity, the gated approach improves the suitability of phosphor thermometry for investigations of fast heat transfer phenomena of industrial relevance.

Acknowledgments

The authors are grateful to the support provided by Robert Bosch GmbH.

ORCID iDs

Aldo Mendieta https://orcid.org/0000-0002-1978-5130
Benoît Fond https://orcid.org/0000-0002-8152-4126
Frank Beyrau https://orcid.org/0000-0002-8043-7194

References

[1] Abram C, Fond B and Beyrau F 2018 Temperature measurement techniques for gas and liquid flows using thermographic phosphor tracer particles *Prog. Energy Combust. Sci.* **64** 93–156
[2] Aldén M, Omrane A, Richter M and Särner G 2011 Thermographic phosphors for thermometry: a survey of combustion applications *Prog. Energy Combust. Sci.* **37** 422–61
[3] Allison S W and Gillies G T 1997 Remote thermometry with thermographic phosphors: instrumentation and applications *Rev. Sci. Instrum.* **68** 2615–50
[4] Binder C, Abou Nada F, Richter M, Cronhjort A and Norling D 2017 Heat loss analysis of a steel piston and a YSZ coated piston in a heavy-duty diesel engine using phosphor thermometry measurements *SAE Int. J. Eng.* **10** 1954–68
[5] Brübach J, Pflitsch C, Dreizler A and Atakan B 2013 On surface temperature measurements with thermographic phosphors: a review *Prog. Energy Combust. Sci.* **39** 37–60
[6] Brutin D, Sobac B, Rigollet F and Le Niliot C 2011 Infrared visualization of thermal motion inside a sessile drop deposited onto a heated surface *Exp. Therm. Fluid Sci.* **35** 521–30
[7] Datcu S, Ibos L, Candau Y and Matteï S 2005 Improvement of building wall surface temperature measurements by infrared thermography *Infrared Phys. Technol.* **46** 451–67
[8] Dragomirov P, Mendieta A, Abram C, Fond B and Beyrau F 2018 Planar measurements of spray-induced wall cooling using phosphor thermometry *Exp. Fluids* **59** 42
[9] Fischer S, Sahu R P, Sinha-Ray S, Yarin A L, Gambaryan-Roisman T and Stephan P 2017 Effect of nano-textured heater surfaces on evaporation at a single meniscus *Int. J. Heat Mass Transfer* **108** 2444–50
[10] Fond B, Abram C, Heyes A L, Kempf A M and Beyrau F 2012 Simultaneous temperature, mixture fraction and velocity imaging in turbulent flows using thermographic phosphor tracer particles *Opt. Express* **20** 22118–33
[11] Fond B, Abram C, Pougin M and Beyrau F 2019 Investigation of the tin-doped phosphor $(Sr,Mg)_3(PO_4)_2:Sn_2$; for fluid temperature measurements *Opt. Mater. Express* **9** 802–18
[12] Fuhrmann N, Brübach J and Dreizler A 2013 On the mono-exponential fitting of phosphorescence decays *Appl. Phys. B* **116** 359–69

[13] Fuhrmann N, Schild M, Bensing D, Kaiser S A, Schulz C, Brübach J and Dreizler A 2011 Two-dimensional cycle-resolved exhaust valve temperature measurements in an optically accessible internal combustion engine using thermographic phosphors *Appl. Phys.* B **106** 945–51

[14] Hasegawa R, Sakata I, Yanagihara H, Aldén M and Johansson B 2008 Quantitative analysis of the relation between flame structure and turbulence in HCCI combustion by two-dimensional temperature measurement, SAE International *Technical Paper* 2008-01-0061 (https://doi.org/10.4271/2008-01-0061)

[15] Hasegawa R, Sakata I, Yanagihara H, Särner G, Richter M, Aldén M and Johansson B 2007 Two-dimensional temperature measurements in engine combustion using phosphor thermometry, SAE International *Technical Paper* 2007-01-1883 (https://doi.org/10.4271/2007-01-1883)

[16] Heichal Y, Chandra S and Bordatchev E 2005 A fast-response thin film thermocouple to measure rapid surface temperature changes *Exp. Therm. Fluid Sci.* **30** 153–9

[17] Husberg T, Gjirja S, Denbratt I, Omrane A, Aldén M and Engström J 2005 Piston temperature measurement by use of thermographic phosphors and thermocouples in a heavy-duty diesel engine run under partly premixed conditions, SAE International *Technical Paper* 2005-01-1646 (https://doi.org/10.4271/2005-01-1646)

[18] Jin D and Piper J A 2011 Time-gated luminescence microscopy allowing direct visual inspection of lanthanide-stained microorganisms in background-free condition *Anal. Chem.* **83** 2294–300

[19] Knappe C, Andersson P, Algotsson M, Richter M, Linden J, Alden M, Tuner M and Johansson B 2011 Laser-induced phosphorescence and the impact of phosphor coating thickness on crank-angle resolved cylinder wall temperatures *SAE Int. J. Eng.* **4** 1689–98

[20] Köpple F, Seboldt D, Jochmann P, Hettinger A, Kufferath A and Bargende M 2014 Experimental investigation of fuel impingement and spray-cooling on the piston of a GDI engine via instantaneous surface temperature measurements *SAE Int. J. Eng.* **7** 1178–94

[21] Le Coz J-F and Baritaud T 1996 Application of laser induced fluorescence for measuring the thickness of evaporating gasoline liquid films *Developments in Laser Techniques and Applications to Fluid Mechanics* Eds R J Adrian, D F G Durão, F Durst, M V Heitor, M Maeda and J H Whitelaw (Berlin: Springer) (https://doi.org/10.1007/978-3-642-79965-58)

[22] Marr M A, Wallace J S, Chandra S, Pershin L and Mostaghimi J 2010 A fast response thermocouple for internal combustion engine surface temperature measurements *Exp. Therm. Fluid Sci.* **34** 183–9

[23] Neal N J, Jordan J and Rothamer D 2013 Simultaneous measurements of in-cylinder temperature and velocity distribution in a small-bore diesel engine using thermographic phosphors *SAE Int. J. Eng.* **6** 300–18

[24] Rodnyi P A and Khodyuk I V 2011 Optical and luminescence properties of zinc oxide (review) *Opt. Spectrosc.* **111** 776–85

[25] Schulz F and Beyrau F 2017 The influence of flash-boiling on spray-targeting and fuel film formation *Fuel* **208** 587–94

[26] Steeper R R and Stevens E J 2000 Characterization of combustion, piston temperatures, fuel sprays, and fuel-air mixing in a DISI optical engine SAE International *Technical Paper* 2000-01-2900 (https://doi.org/10.4271/2000-01-2900)